51st AIAA Aerospace Sciences Meeting including the New Horizons Forum and Aerospace Exposition
07 - 10 January 2013, Grapevine (Dallas/Ft. Worth Region), Texas

AIAA 2013-0233

Shape Design to Minimize the Peak Heat-Flux of Blunt Leading-Edge

Kai Cui*, Shou-Chao Hu
State Key Laboratory of High-temperature Gas Dynamics, Institute of Mechanics, Chinese Academy of Sciences, Beijing, 100190, China
**Corresponding author: kcui@imech.ac.cn*

To minimize the peak heat-flux of hypersonic blunt leading-edge, the Mini-Max optimization model is introduced for the first time for aerothermodynamics optimization. The surface heat-flux is obtained by resolving Navier-Stokes equations, and only the frozen flow is considered. The computational fluid dynamics (CFD) based Genetic Algorithm is used as the optimizer. A novel 2-D profile of leading-edge is obtained and the peak heat-flux is significantly reduced. Compared to the commonly used circular leading-edge, there is a large area of high temperature, high pressure in the front part of leading-edge, together with greater shock stand-off distance. The thickness of thermal boundary layer is increased about 40% at the stagnation point, the peak heat-flux is decreased about 20% and the heat-flux distribution is little changed in the vicinity of stagnation point. The robustness analysis shows that the favorable performance of the optimal 2-D profile is universally effective, i.e., it can effectively decrease the peak heat-flux by about 20% for various wall temperatures, Mach numbers, flight altitudes and thicknesses of the leading-edge as compared with the corresponding case of circular leading-edge. Although the reduction scope of peak heat-flux decreases with the change of angle-of-attack, but the peak heat-flux can still be decreased by more than 4% when the angle-of-attack is not greater than 15°. Several axisymmetric cases are also investigated in this paper, and the circular cone is taken as the benchmark, the peak heat-flux around an axisymmetric blunt cone, which is generated by the corresponding optimal 2-D profile, is also reduced by about 25%. Similarly, the distribution of heat-flux around the stagnation point is almost unchanged.

Nomenclature

C_p	=	pressure coefficient
D	=	thickness of the leading-edge/nose-tip
H	=	flight altitude
h_0	=	total enthalpy
h_w	=	wall enthalpy
h_∞	=	enthalpy of the free-stream flow
Ma_∞	=	flight Mach number
P	=	pressure
Q	=	heat-flux
Q_0	=	heat-flux of the stagnation point
Q_{max}	=	peak heat-flux
$Q(x)$	=	heat-flux along the leading-edge
R_0	=	curvature radius at the stagnation point
T	=	temperature
T_w	=	wall temperature
V_∞	=	velocity of the free-stream flow
α	=	angle-of-attack
θ	=	the induced angle with respect to the x-axis
φ	=	angle between a tangent to the surface and the free-stream direction
ρ_∞	=	density of the free-stream flow
Δy_n	=	grid thickness for the first layer near the wall

I. Introduction

Hypersonic vehicles are always designed with sharp leading-edge or sharp nose-tip to effectively reduce the drag caused by strong shock-wave and to raise the lift-drag ratio of vehicles. With the 'wave-rider' configuration as an example, the theoretical perfect lift-drag ratio can be obtained only by designing sharp leading-edge with no thickness [1-3]. However, sharp leading-edges or nose-tips are exposed to severe heating while flying at high Mach number. To reduce the severe drag force and heat-flux, lots of novel attachments, such as spiked nose-tip, opposing jet flow from the nose-tip, forward-facing cavity etc. have been proposed by scientists. It can actually be interpreted as increasing the slenderness ratio of bunt body when a needle-liked body[4-6] or opposing jet flow[7-9] is mounted at the nose tip. The pressure and temperature decrease significantly while the strong bow shock wave is weakened to several oblique shock waves associated with the increase of slenderness ratio. In addition, the severe aerodynamic heating can also be reduced by the circulation region formed in front of the blunt body[6]. A forward-facing cavity in the nose-tip is known to cause bow shock oscillations[10, 11]. The flow within the cavity would be oscillating (unsteady movement of shock within the cavity). If an appropriate cavity configuration is chosen, the mean surface heat-flux would be reduced because lots of heat would be taken away by the process of 'swallow' and 'spitting' caused by the oscillations[12, 13].

Given the effectiveness of trade-off between aerodynamic forces and aerothermodynamics and the potential applications, it is worthy to conduct some in-depth studies on the adoption of attachments mentioned above. However, adoption of attachments leads to more complex design of vehicles, for example, the structural strength problems for spikes and the jet devices design for opposing jet must be considered. In addition, attachments in front of the vehicles makes the flow-field much more complicated, such as the circulation region caused by spikes or opposing jets and the shock wave oscillation caused by forward-facing cavity. Given that the aerodynamic performance of 'wave-rider' or X-51A liked air-breathing hypersonic vehicles is sensitive to the change of flow-field, the direct blunting technique, which is also the simplest technique, is most commonly used for aero-thermal protection of hypersonic vehicles.

As for the heat-flux of stagnation point (which is always the position where peak heat-flux is located), theoretical self-similar solutions[14-17], experiment results[18, 19]and some semi-empirical analyses[20-22] have all supported that it is inversely proportional to the root of curvature radius at the stagnation point,

$$Q_0 \propto 1/\sqrt{R_0} \qquad (1)$$

which is also the theoretical basis of direct blunting technique for aero-thermal protection. Obviously, greater blunt radius (or thickness of the nose-tip/leading-edge) leads lower heat-flux value at the stagnation point which makes the vehicle safer, whereas it also results in higher drag force, especially the increase of shock resistance. Traditionally, it needs a trade-off between the drag and the aero-thermal protection to choose an appropriate blunt radius (or thickness of the nose-tip/leading-edge), but the aero-thermal protection is preferred as far as security is concerned. So the nose-tip/leading-edge of hypersonic vehicles must be thick enough to survive the severe aerodynamic heating. For the most commonly used power-law shape and circular leading-edge, the peak value of heat-flux is located at the stagnation point, and the thicker the nose-tip/leading-edge, the lower the peak heat-flux. However, thin leading-edge is also needed for both achieving well riding on the shock-wave for 'wave-rider' and obtaining satisfactory flow-field in front of the engine inlet for air-breathing hypersonic vehicles.

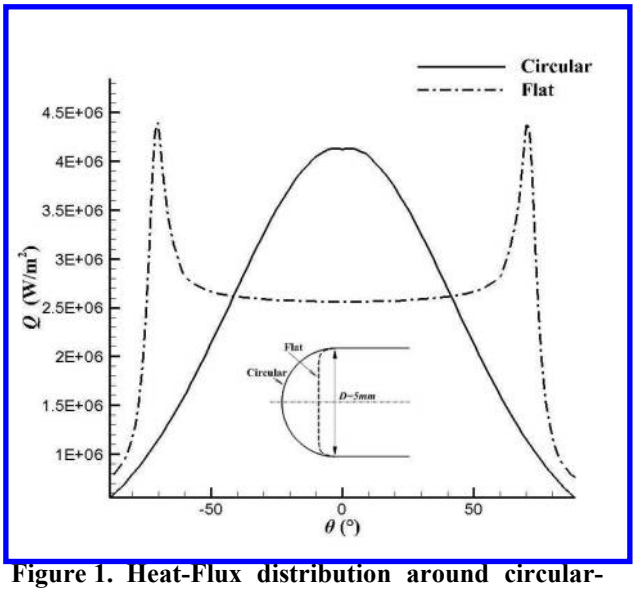

Figure 1. Heat-Flux distribution around circular-leading-edge and flat-leading-edge.

The heat-flux distribution (or the distribution of energy injection) is non-uniform along the nose-tip/leading-edge which is shaped by a power-law curve or a circular curve. The distribution can be characterized with its peak value located at the stagnation point and the value decreasing along the leading-edge with increasing distance from the stagnation point. Therefore, an intuitionistic idea would be proposed that the heat-flux distribution can be modified to further decrease the peak value by changing the shape of nose-tip/leading-edge with limited thickness of nose-tip/leading-edge. A simple simulation test has been

done to verify the idea as follows. The surface heat-flux of 2-D circular leading-edge and 2-D chamfered flat leading-edge were obtained by numerical simulation, in which the thickness of leading-edges was both limited to 5mm (the corresponding radius of circular was 2.5mm). The results (the similar heat-flux distributions of circular and chamfered flat leading-edges are also supported by experiment data[17] and theoretical solution based on local similarity [15-17]) are shown in Figure 1.

As shown in Figure 1, compared to the ordinary circular leading-edge, the heat-flux at the stagnation point can be significantly reduced (about 40%) when the curvature radius increases to the upper limit (corresponding to the case of flat leading-edge). However, the heat-flux increases rapidly at the chamfer of the flat leading-edge since the curvature radius there is much smaller than the radius of circular leading-edge, and the peak heat-flux of the chamfered flat leading-edge would be even higher than that of the circular-arc. From this simple test, at least two conclusions can be drawn as follows. 1) It's practicable to modify the heat-flux distribution via deforming the shape of the nose-tip/leading-edge, and the peak heat-flux can probably be decreased with fixed thickness of nose-tip/leading-edge. 2) The peak heat-flux may be not located at the stagnation point but at other point where the curvature radius is smaller as the shape of nose-tip/leading-edge is changed. In addition, the location of the peak heat-flux is difficult to be determined in advance as the curvature is different for different line shape.

Based on the above-mentioned, the main purpose of this paper is to find a new shape line of leading-edge which is characterized with lower peak heat flux and relatively more uniform distribution compared with the case of circular leading-edge. A combination of numerical simulation and nonlinear optimization method has been employed. On the premise of keeping smoothness of the leading-edge profile, the B-spline curve that can simply change the curve shape by local modification was used for the parametric design of leading-edge. Besides, the point of peak heat-flux may be located at any points along the leading-edge rather than just on the stagnation point, so the main difficulty of this work is that the optimization objective cannot be expressed by a continuous function. The Mini-Max optimization model, in which the optimization objective is set to be the minimum peak heat-flux of the leading-edge, is introduced for the first time to address this problem. The Mini-Max model can be vividly described as 'Suppressing the peak point'. The procedure of 'Suppressing the peak point' is not only reflected in 'suppressing (or pressing down)' the peak value of the heat-flux, but also reflected in 'suppressing (or planishing)' the locally sharp convex region to increase the curvature radius. In view of the discontinuity of the optimization objective, Genetic Algorithm is also adopted in this paper to search for the optimal shape [23].

Based on the above ideals, an optimized 2-D profile of leading-edge with the thickness of 5mm has been designed under the condition of ideal-gas. An impressive profile of leading-edge is obtained in this work. As compared to the commonly used circular leading-edge, the peak heat-flux has dramatically been reduced by about 20%, and it is universally valid for different wall temperatures (300K~1800K), flight altitudes (20Km~40Km, corresponding to the unit Reynolds number of $4.95E5m^{-1}$ ~ $1.19E7m^{-1}$) and Mach numbers (4~12). The optimal shape can be simply scaled to match various thicknesses of leading-edge, and the peak value of heat-flux is also decreased by about 20% as compared to the corresponding case of circular leading-edge. The reduction of the peak heat-flux decreases with increasing angle-of-attack, but the peak heat-flux are still lower than that of the circular leading-edge when the flight angle-of-attack is not greater than 15°. In addition, as the heat-flux distribution of axisymmetric cone is of similar pattern to that of the 2-D cylinder, the effectiveness of axisymmetric model has been validated for the optimal profile with respect to the circular one. The results shows that the optimal profile can also be used to reduce the peak heat-flux of revolution bodies, and the peak heat-flux is decreased by 25%~30% as compared to the corresponding case of circular cones.

The present paper is organized as follows. Section II describes the optimization model and the procedure of optimization, B-spline parametric design of the profile of leading-edge and the simulation model and grid convergence tests are also discussed. The numerical results are presented and discussed in Section III. The robustness of the results is discussed for various wall temperatures, flight Mach numbers, flight altitudes, attack angles and thicknesses of leading-edge in Section IV. The validity for axisymmetric model is discussed in Section V, and summary and conclusions are finally drawn in Section VI.

II. Optimization Approach

A. Optimization Objective and Procedure

The target of this work is to obtain an optimal 2-D profile of leading-edge which is characterized with appropriate heat-flux distribution. The objective of the optimization is to minimize the peak heat-flux, which can be expressed in the Mini-Max model as follows,

$$\min_{x \in R} \{\max Q(x)\} \qquad (2)$$

where x denotes for design variables, $Q(x)$ denotes for the heat-flux values along the leading-edge obtained by numerical simulation. Figure 2 shows the procedure of the optimization, including three steps as follows.

1) Parametric design of the leading-edge. It means representing the profile of leading-edge by several parameters (design variables) so that the profile can be modified by just changing the value of parameters. A good parametric design method should properly represent the geometry shape according to the physical characteristic of the problem by using as few design variables as possible. B-spline interpolation design method can represent complex curves by a few control points. And the good feature of local modification of B-spline interpolation is quite suitable for the "suppressing the peak point" type of design (to flatten the zone with smaller curvature radius, so that the heat-flux decreases with increasing curvature radius). Besides, the smoothness which is quite important for the profile of leading-edge is guaranteed by using the B-spline interpolation. So, the B-spline interpolation method is used here for the parametric design of leading-edge with details presented in §B.

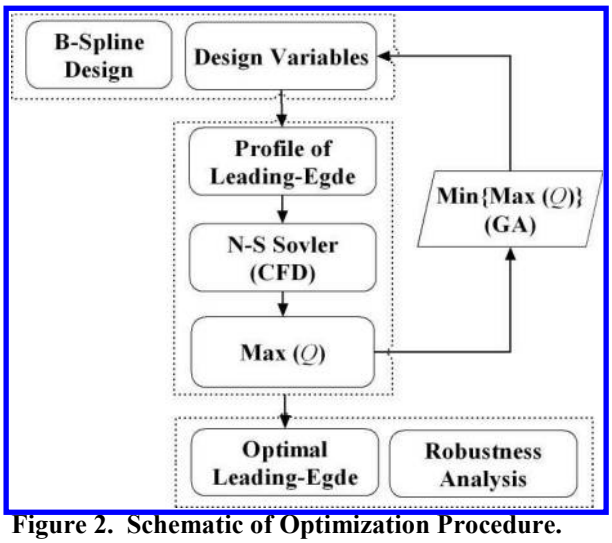

Figure 2. Schematic of Optimization Procedure.

2) Solution of the Mini-Max optimization problem. The surface heat-flux of the leading-edge can be obtained by numerical simulation (§C), and the peak value should be taken as the objective. As mentioned above, the peak value may be located anywhere around the leading-edge, and as a result the objective function is discontinuous or even transilient. So, it is impossible to get the gradient value of the objective function. The Genetic Algorithm, stochastic optimization method rather than gradient-based method is used in this study.

3) Robustness analysis of the optimal leading-edge. The optimization design in step 2 is just for the design point (D=5mm, Ma_∞=6.5, H=25Km, T_w=300K), but only an optimal profile with good robustness can be of great practice significant. So a detailed robustness analysis will be performed in section 4 to verify the universal effectiveness of the optimal profile.

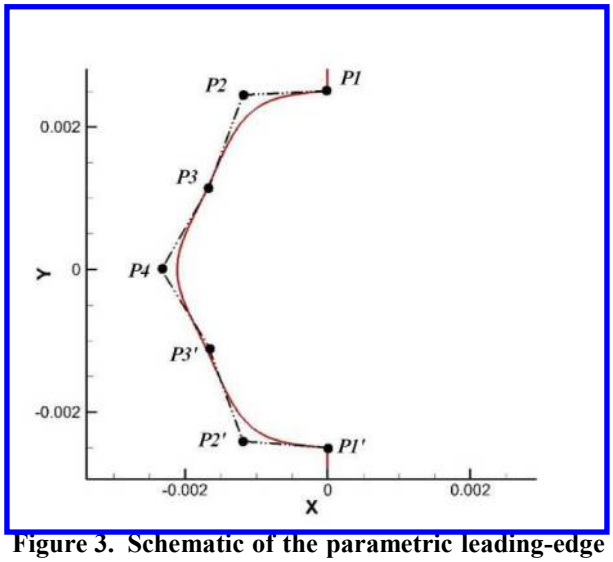

Figure 3. Schematic of the parametric leading-edge (7 control-points and 5 design-variables were involved).

B. Parametric Methodology

Figure 3 shows the parametric design of leading-edge by using subsection cubic B-spline interpolation. Seven control points, P1~P4 and P1'~P3' are used for the B-spline, as shown in Figure 3. Here, the coordinate values of P1 and P1' are determined by the thickness of the leading-edge. As the leading-edge is up-down symmetry, the x coordinate value of P4 is determined to be zero, and P2', P3' are set to be the symmetry point relative to the Y-coordinate-axis of P2 and P3, respectively. And thus the profile of the leading-edge is finally parameterized by five design variables only, as shown in Table 1.

Table 1 Design variables' description

Design variable	ranges	description
V1	[-1.5,-0.5]	x coordinate value of P2
V2	[1.8,2.5]	y coordinate value of P2
V3	[-3.0,-1.5]	x coordinate value of P3
V4	[0.5,1.8]	y coordinate value of P3

V5	[-3.0,-0.5]	x coordinate value of P4

C. Numerical Methodology

The code used in this study is a turbulent two-dimensional full Navier-Stokes code utilizing Advection Upstream Splitting Method(AUSM+) and implicit time-marching, and a k-□-R_t model was used to predict the turbulent flow. At the design point, the ambient conditions was corresponding to the ideal-gas (only frozen flow is considered in this study) at 25Km standard altitude, the thickness of leading-edge was chosen to be 5mm, the wall temperature was set to 300K, the flight Mach number was chosen to be 6.5 and the kinematical viscosity coefficient was obtained by Sutherland formula.

In the hypersonic flight regime, the blunt body generates a strong detached bow shock wave ahead of it. The shock wave is responsible for the elevated levels of pressure and aero-heating in downstream flows, and a mass of heat exchange take place between the high temperature atmosphere and blunt body at the bottom of the viscous layer. Thus, a refined grid is needed to get accurate heat-flux value by accurately simulating the flow filed of viscous boundary layer. The heat-flux is proportional to the temperature gradient,

$$Q = k\left.\frac{\partial T}{\partial n}\right|_w \qquad (3)$$

Especially, the grid thickness should be thin enough for the first layer near the wall Δy_n so as to accurately simulate the temperature gradient and heat-flux. Before the optimization, a grid convergence has been tested for the surface spacing Δy_n around the circular leading-edge. Four types of grid distribution was chosen for the test, the gird dimension were all set to 101×151 (circumferential-direction × normal-direction), and $\frac{D}{2}\times10^{-2}$, $\frac{D}{2}\times10^{-3}$, $\frac{D}{2}\times10^{-4}$, $\frac{D}{2}\times10^{-5}$ is chosen for Δy_n respectively. The results (Figure 4) shows that the calculation error is less than 1% when Δy_n is smaller than $\frac{D}{2}\times10^{-3}$. For the subsequent simulations, the Δy_n is set to $\frac{D}{2}\times10^{-5}$ and the corresponding $\Delta y_n^+ < 0.1$. Figure 5 illustrated the grid and computation domain.

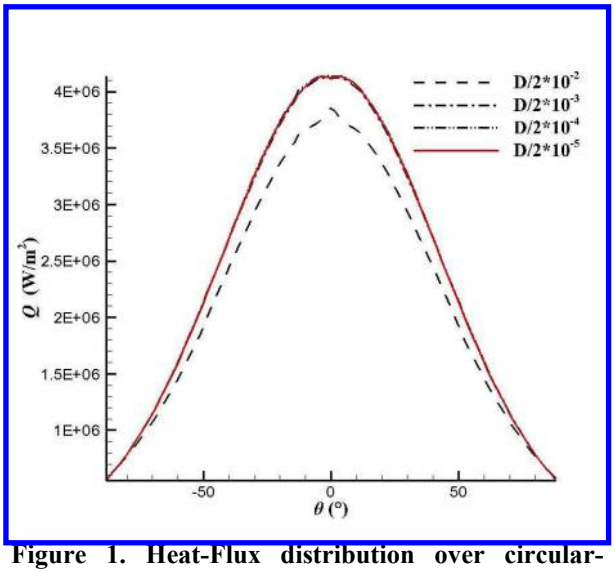

Figure 1. Heat-Flux distribution over circular-leading-edge for various surface grid fineness levels.

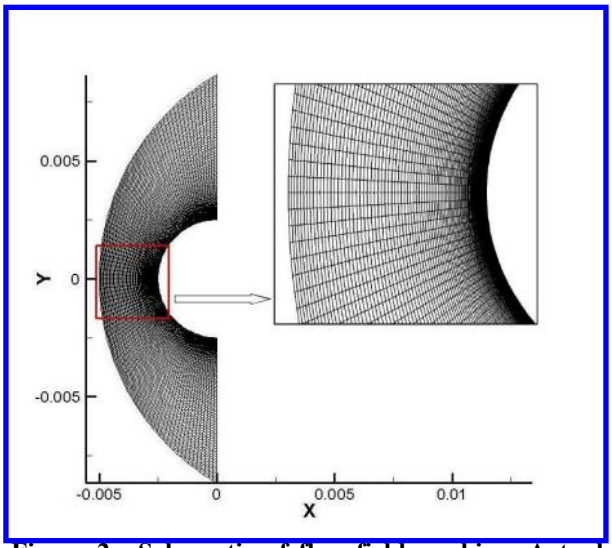

Figure 2. Schematic of flow-field meshing. Actual surface spacing at the leading-edge was D/2×10⁻⁵.

III. Numerical Results and Analysis

A. Aerodynamic Heating and Force

Genetic Algorithm have the capability of finding out the global optimum value by mimicking the inherence and variation characteristic of biological reproduction in the iterative optimization process. Here, double vector code is adopted, the population size and generation number is set to 10 and 30, respectively, 2 elites of each generation are preserved, the crossover probability is set to 0.8 and the Gaussian variation function is used. The objective function (Figure 6) and the profile of leading-edge (Figure 7) are gradually approaching the target after 300 times iterations. Figure 7 illustrates the circle and the optimum shapes of the first, seventeenth, and thirtieth (which is also the final optimum profile) generation.

The numerical results of both the Baseline (circular)

and the optimal leading-edges are presented and compared in Table 2 and Figure 8. The peak heat-flux is reduced by about 20% when compared to the circular leading-edge. Laminar based simulation results are also included in Table 2, the peak values decrease for both the circular and the optimal leading-edges as compared to the results obtained for turbulence flow, but the peak heat-flux of the optimal leading-edge can still be reduced by about 21% when compared to that of the circular leading-edge. The optimal profile looks 'blunter' than circular (Figure 7). The surface heat-flux near the stagnation point has been dramatically reduced though it increases in the area of $|\theta|>30°$ (θ is the induced angle with respect to the X-axis). In addition, the distribution of heat-flux is almost uniform in the region of $|\theta|<50°$ (Figure 8). To sum up, the optimal profile is characterized with a reasonable heat-flux distribution that is kept nearly at a constant value in the vicinity of stagnation point ($|\theta|<50°$), and the peak value is dramatically reduced though the sum of the surface heat-flux is almost unchanged.

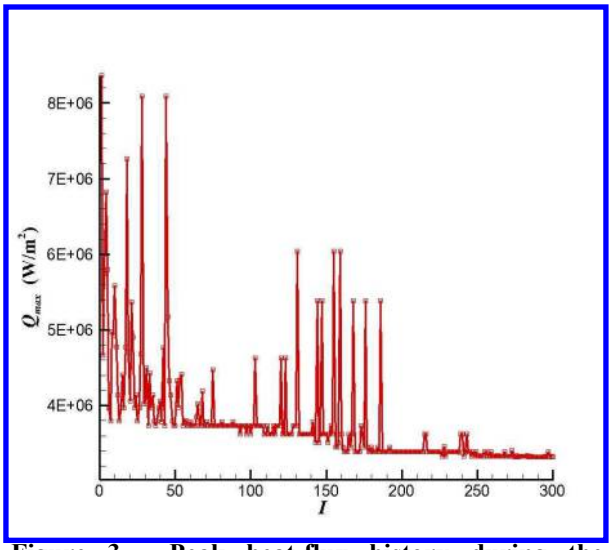

Figure 3. Peak heat-flux history during the optimization process.

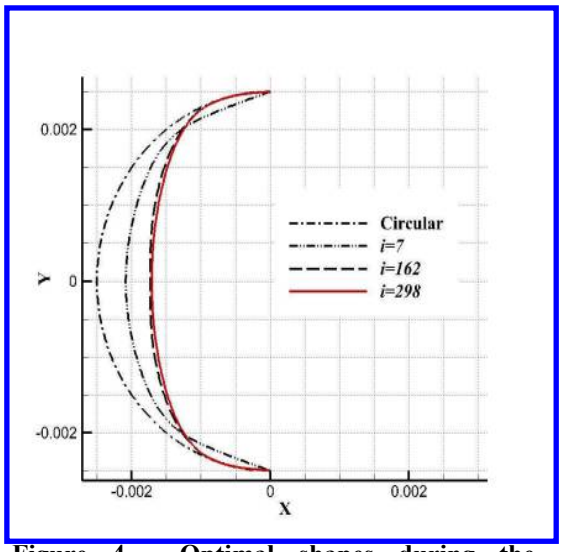

Figure 4. Optimal shapes during the optimization process.

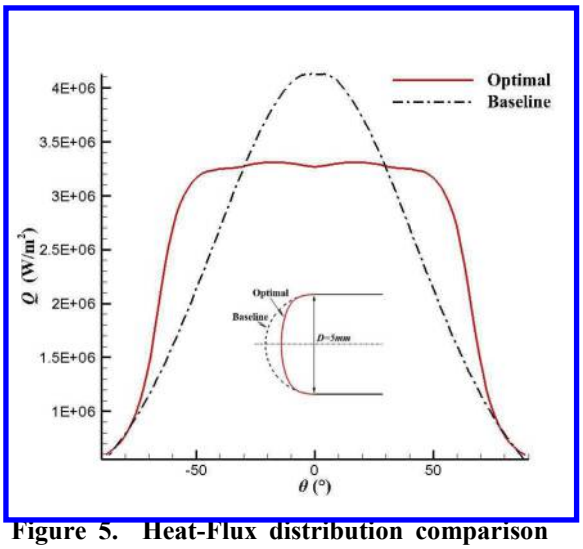

Figure 5. Heat-Flux distribution comparison between Baseline(dashed line) and Optimal leading-edge(solid line).

Table 2 Numerical results comparison between the Baseline and the Optimal leading-edge

	Turbulence model	Wall Boundary	Baseline	Optimal	Reduced by
Q_{max}(W/m^2)	*k-ε-Rt*		4132495.5	3308691.5	+20%
	Laminar	T_w=300K	3579340.3	2828422.5	+21%
Drag coefficient	*k-ε-Rt*		1.3005	1.4545	-12%
T_{max}(K)	*k-ε-Rt*	Adiabatic	2120.3	2118.3	+0.01%

The well-known Newtonian law points out that the pressure coefficient is proportional to sine-squared,

$$C_p = 2\sin^2\varphi \qquad (4)$$

where φ is the angle between a tangent to the surface and the free-stream direction. There's a greater φ near the stagnation zone ($|\theta|<50°$) as the optimal profile is 'blunter' than that of the circle arc. Thus, the pressure coefficient around the leading-edge increases (Figure 9), and the total drag coefficient of the optimal 2-D leading-edge increases by about 12% (Table 2).

Although the heat-flux near the stagnation point is dramatically reduced, the peak temperature of the leading-edge obtained by numerical simulation with an adiabatic (no heat exchanging) wall boundary condition is unchanged (Table 2). On the contrary, the wall temperature increases near (but not on) the stagnation point since the optimal profile is 'blunter' (Figure 10). Obviously, the severe high temperature environment downstream of the bow shock cannot be changed by just modifying the profile of leading-edge, but the heat-flux distribution can be modified and the peak heat flux can be reduced. Considering the most widely and successfully used ablative thermal protection technology, it is worthy to point out that the modified heat-flux distribution yields relatively uniform heat transfer in the most severe aero-heating zone (in the vicinity of stagnation point), which helps to stabilize the geometry shape as much as possible because of uniform ablation.

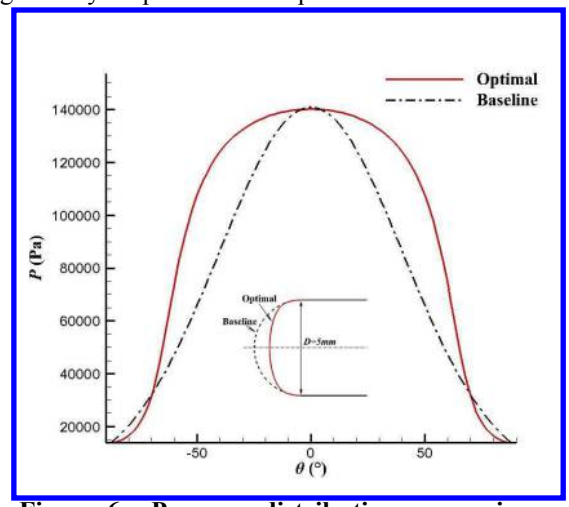

Figure 6. Pressure distribution comparison between Baseline(dashed line) and Optimal leading-edge(solid line).

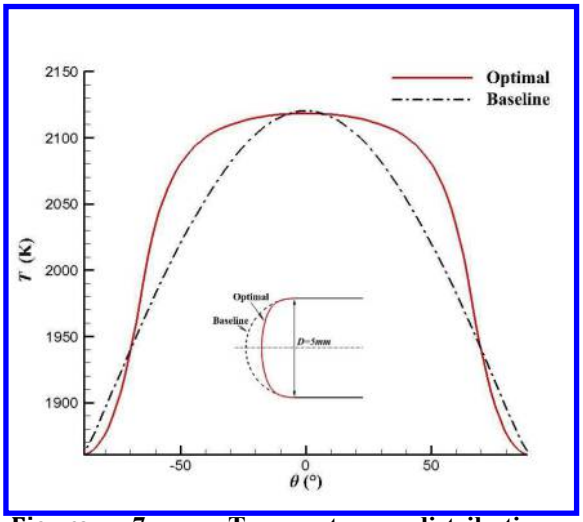

Figure 7. Temperature distribution comparison between Baseline(dashed line) and Optimal leading-edge(solid line).

B. Profile of The Optimal Leading-Edge

The optimal profile is flatter than the circle near the stagnation point (Figure 7). And it is characterized with greater curvature radius than the corresponding circle in the zone of $|\theta| \in (50°,80°)$(Figure 11, the curvature is reciprocal to the curvature radius, and the curvature of 5mm diameter circle corresponds to a constant value of 400m-1). The curvature which experiences a first increasing and then decreasing in the zone of $|\theta| \in (50°,80°)$ is smaller than that of circle. The maximum curvature is located at the point where $|\theta|$ is about 65°, and corresponds to the minimum curvature radius which is almost one-third of that of the corresponding circle.

Although the minimum curvature radius of the optimal profile is nearly one-third of the corresponding circle's, it would not lead to a great heat-flux value because it is located at the point of $|\theta|$=65°. Compared to that in the vicinity of stagnation point, the severe aero-heating has been weakened in the zone of $|\theta| \geq 65°$. The induced angle φ between the tangent to the surface and the free-stream direction is greatly reduced, resulting in lower pressure coefficient and temperature near the wall (Figure 9，Figure 10).

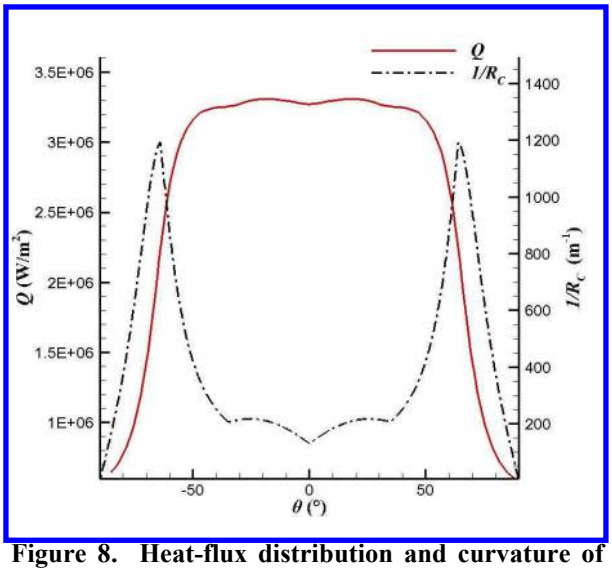

Figure 8. Heat-flux distribution and curvature of the Optimal profile.

It claims attention that the stagnation point is moved when the free-streams is at non-zero angle-of-attack, and the heat-flux would dramatically increase as the stagnation point moves to a zone of smaller curvature radius. The

influence of angle-of-attack has been discussed in §D, and the results shows affirmatively that the peak heat-flux has been reduced by more than 4% when the angle-of-attack is not greater than 15°.

C. Structures of Flow Field

The hypersonic free-stream flow generates a strong detached bow shock in front of the 2-D cylinder leading-edge. The velocity of flow downstream of the shock wave slows down rapidly, and the statistic temperature and statistic pressure increase suddenly. It constitutes a stagnation region characterized with high temperature, high pressure and low speed flow in front of the stagnation point (Figure 12~Figure 14). There's a larger stagnation region since the optimal profile is 'blunter' than the circle arc. Thus, the wall pressure and temperature (obtained by adiabatic wall boundary condition) near the stagnation point is greater than that of the circle arc (Figure 9, Figure 10). The position of shock-wave moves slightly forward, but the shock stand-off distance increases since the optimal profile is much 'blunter' than the circle (Figure 13). In addition, enlarged stagnation region leads to change of shape of the shock wave, the angle of shock wave (the angle between the tangent to the shock wave and the axis of the shock) increased slightly, and as a result the shock stand-off distance also increases in other parts of the leading-edge (Figure 13).

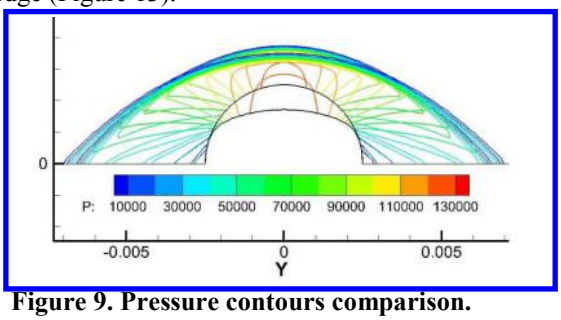

Figure 9. Pressure contours comparison.

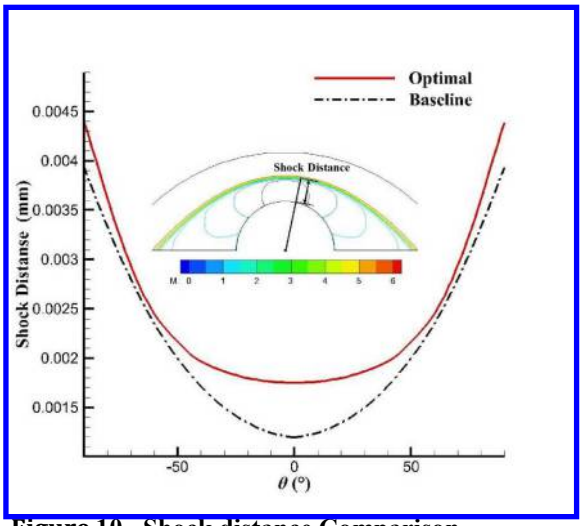

Figure 10. Shock distance Comparison.

The increases in stagnation flow area and shock stand-off distance have greatly influenced the thickness of the viscous boundary layer. Once the free-stream flow condition is determined, the statistic temperature of stagnation point is fixed to the total temperature of free-stream and cannot be decreased by direct blunting techniques. The numerical results comparison, as given in Table 2 and Figure 14, shows that the temperature of stagnation point and the edge temperature of thermal boundary layer in the vicinity of stagnation point are unchanged. But then the thickness of thermal boundary layer increases dramatically as the stagnation flow area has been greatly enlarged and the shock stand-off distance has increased. As shown in Figure 14, the thickness of thermal boundary layer of the optimal and circular 2-D leading-edge is 7.1×10^{-5}m and 5.1×10^{-5}m, respectively, i.e. it is increased by about 40%. Thus, the temperature gradient within the thermal boundary layer decreases, and the value of heat-flux decreases accordingly.

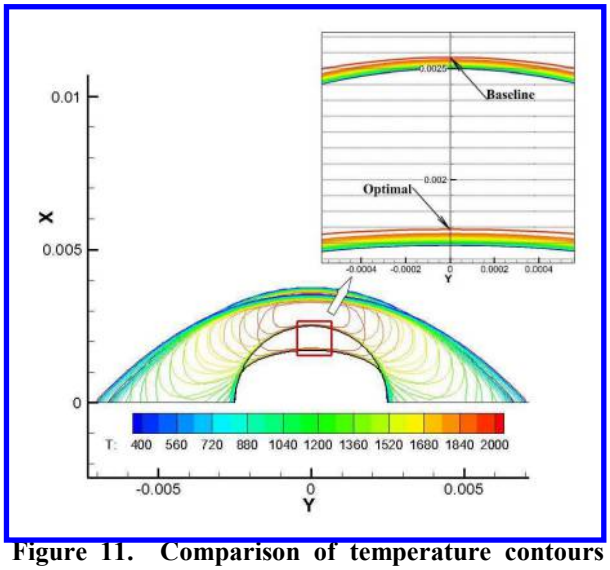

Figure 11. Comparison of temperature contours and thickness of thermal boundary layer.

Besides, due to the 'bluntness' of the optimal profile and the enlargement of the high temperature flow area, both the thickness and edge temperature of thermal boundary layer is nearly unchanged in the vicinity of the stagnation point ($|\theta| \in (0°,50°)$), and as a result, the

temperature gradient within the thermal boundary layer and the value of heat-flux is unchanged accordingly (Figure 8).

IV. Robustness of the Optimal Leading-edge

The optimal leading-edge behaves well at the design point regarding aero-thermal protection, but for promotion and application of the optimal profile, it is most important for the profile to possess good robustness. As illustrated in Figure 8, the peak heat-flux of the optimal leading-edge approximates to the value at stagnation point as the values in the zone of $|\theta| \in (0°,50°)$ are nearly unchanged. Besides, the peak heat-flux of circular leading-edge is also located at the stagnation point. Thus, it is helpful to sort out the main factors by analyzing the heat-flux of stagnation point, which makes the robustness analysis 'targeting'. For the heat-flux of stagnation point, lots of theoretical, experiments and semi-empirical solutions have been derived, among which the most famous is the semi-empirical formula obtained by J.D. Anderson etc. [21], which reads

$$Q_0 \propto (1-\frac{h_w}{h_0}) \cdot \rho_\infty^{\frac{1}{2}} \cdot V_\infty^3 \cdot R_0^{-\frac{1}{2}} \qquad (5)$$

where

$h_w = C_{pw} T_w$

$h_0 = h_\infty + V_\infty^2 / 2$

Accordingly, the wall enthalpy h_w, total enthalpy of the free-stream flow h_0, density of the free-stream flow ρ_∞, velocity of the free-stream flow V_∞ and the curvature radius of the stagnation point R_0 would be specifically selected for the robust analysis.

Here, taking the practical engineering background into consideration, the robust analysis for the aero-thermal protection of optimal leading-edge is organized as follows, 1) Investigation on the wall enthalpy h_w has been carried out by changing the wall temperature T_w(300K~1800K) in section A. 2) Investigation on the total enthalpy h_0, density ρ_∞ and velocity V_∞ of the free-stream flows has been carried out for various flight altitudes H(20Km~40Km) and Mach numbers Ma_∞(4~12) in section B. As the flight altitude increases from 20Km to 40Km, there's a significant change of ρ_∞ (about twenty three fold), and V_∞ and h_0 also changes a little due to temperature change thereby. On the other hand, the change of Mach number mostly affects V∞, and h0 also changes a little due to the change of V_∞. 3) Investigation on curvature radius R_0 has been carried out in two parts, the effect of thickness of the leading-edge D (5mm~40mm) and that of angle-of-attack α (0°~30°), as discussed in section C and section D, respectively. The size of the leading-edge needs to be scaled as the thickness of leading-edge changes, and R_0 is scaled correspondingly. On the other hand, the stagnation point would move because of change of attack angle, and R0 would also be changed, as shown in Figure 11, where the curvature distribution of the optimal profile is non-uniform, and thus the movement of stagnation point would result in an increase of peak heat- flux.

A. Wall Temperatures

Under condition of H=25Km, Ma_∞=6.5, D=5mm, α=0°, six cases with different wall temperatures has been studied to verify the aero-thermal protection performance of the optimal leading-edge. The temperature difference between the wall and thermal boundary outer-edge decreases as the temperature of isothermal wall increases, which leads to a reduction of temperature gradient and correspondingly, a decrease of heat-flux. The reduction proportion of heat-flux is nearly the same in both the optimal and the circular leading-edge cases, and the heat-flux distribution is both similar to that shown in Figure 8. The peak heat-fluxes are steadily decreased by about 20% as compared to that of the circular leading-edge (Table 3).

Table 3 Comparison of peak heat-flux for various wall temperatures

Wall Temperature(K)	Baseline	Optimal	Reduced by
300	4132495.5	3308691.5	+20%
600	3473824.5	2785081.3	+20%
900	2796267.0	2229367.8	+20%
1200	2113293.0	1692545.9	+20%
1500	1425652.4	1139362.5	+20%
1800	736821.2	584651.4	+21%

B. Flight Altitudes and Mach Numbers

Under the condition of T_w=300K, Ma_∞=6.5, D=5mm, α=0°, six cases with different flight altitudes ranging from 20Km to 40Km has been studied to verify the aero-thermal protection performance of the optimal leading-edge. The gas state parameters are obtained from the international standard atmosphere list, here, the unit Reynolds number spans two orders magnitude(from $4.95\times10^5 m^{-1}$ to $1.19\times10^7 m^{-1}$, Figure 15). As the flight altitude increases, the density of the atmosphere and the unit Reynolds number decreases, and the heat-flux decreases accordingly. The heat-flux distribution in these cases is similar to that at the design point shown in Figure 8. The reduction of peak-heat flux increases slightly as the flight altitude increases, and the peak value is reduced by about 20% compared to the corresponding case of circular leading-edge (Table 4).

Table 4 Comparison of peak heat-flux for various flight altitude values

Altitude(Km)	Circular	Optimized	Reduced by
20	6111139.0	4905992.0	+20%
23	4824684.5	3880997.8	+20%
25	4132495.5	3308691.5	+20%
30	2838345.3	2255883.8	+21%
35	2062320.6	1608656.8	+22%
40	1596527.8	1222057.8	+23%

Under the condition of T_w=300K, H=25Km, D=5mm, α=0°, several cases with different flight Mach numbers ranging from 4 to 12 has been studied to verify the aero-thermal protection performance of the optimal leading-edge. For Ma_∞=10, the maximum temperature would be higher than 4000k if the ideal-gas model is used, and this high temperature would lead to ionization of Oxygen and Nitrogen molecules and the ideal-gas model without considering the real gas effects would not be suited to evaluate the heat-flux at the leading-edge. But then the impact of real gas effects on aero-heating and thermal boundary layer is not the focus of this study. Although it is not quite reasonable to evaluate the heat-flux by using the frozen flow model at Mach 10 and 12, it's feasible to verify the effects of velocity on the aero-thermal protection of the optimal leading-edge.

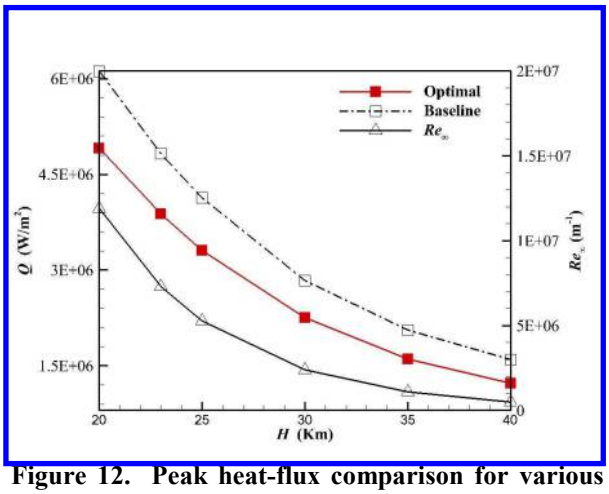

Figure 12. Peak heat-flux comparison for various flight altitude and Re$_\infty$.

As Ma_∞ increases, the velocity and unit Reynolds number of free-streams increases linearly, and the total enthalpy h_0 increases quadratically. The heat-flux is proportional to h_0 and to the cube of V_∞, and thus it increases rapidly as both h_0 and V_∞ increases (Equation (5)). The increment proportion of heat-flux is nearly the same in both the optimal and the circular leading-edge cases, and the optimal leading-edge exhibits a good performance of aero-thermal protection. The heat-flux distribution is both similar to that shown in Figure 8. The peak heat-flux are steadily decreased by about 20% as compared to that of the circular leading-edge (Table 5).

Table 5 Comparison of peak heat-flux for various flight Mach numbers

Ma$_\infty$	Circular	Optimized	Reduced by
4	835783.6	677299.9	+19 %
6.5	4132495.5	3308691.5	+20%
8	8001004.5	6388588.5	+20%
10	16108993.0	12837634.0	+20%
12	28288982.0	22550940.0	+20%

C. Thickness of The Leading-Edge

The thickness of hypersonic vehicles' leading-edge is constrained by both aero-thermal protection and aerodynamic performance. Even for the same aircraft, the thickness of leading-edge is different for different parts of the aircraft, so the optimal leading-edge profile need be scaled to match the size of the thickness of leading-edge.

and thus scaling the leading-edge is also an important indicator for the robustness verification. Under the condition of design point Tw=300K, H=25Km, Ma∞=6.5, α=0°, four cases with different size of the leading-edge has been studied. The peak heat-fluxes of both the optimal and circular leading-edges are changed proportionally. The surface heat-flux distribution is similarly to that shown in Figure 8, and the peak value in the optimal case is decreased by about 20% as compares to the case of circular leading-edge (Table 6).

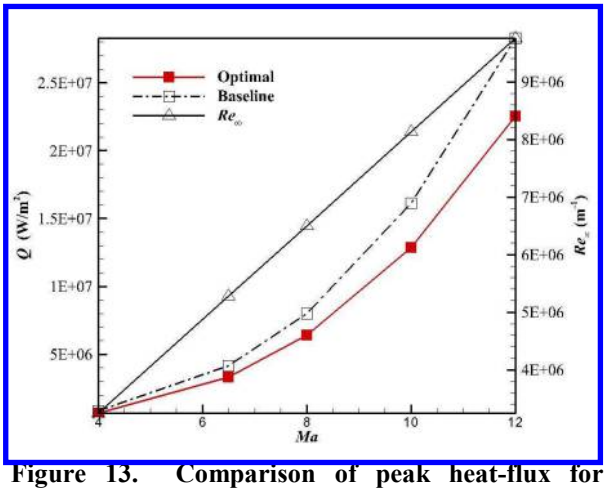

Figure 13. Comparison of peak heat-flux for various Ma_∞ and Re_∞.

Table 6 Comparison of peak heat-flux for various thickness values

Thickness(mm)	Baseline	Optimal	Reduced by
5	4132495.5	3308691.5	+20%
10	3005784.5	2413445.5	+20%
20	2186993.5	1757907.8	+20%
40	1591611.4	1276121.9	+20%

D. Angle-of-Attack

The stagnation point may be located at certain place with smaller curvature radius when it moves with the change of angle-of-attack, and the peak heat-flux increases correspondingly (Equation (5)). The peak heat-flux of circular leading-edge (located at the stagnation piont) is unchanged when the angle-of-attack changes, because its curvatur radious is constaint, equal to half of the thickness. While the peak heat-flux increases with the angle-of-attack increases for the optimal leading-edge (Table 7). When the angle-of-attack is greater than 20°, the heat flux increases rapidly due to the much smaller curvature radius in the zone of $\theta \in$(-70°,-50°), and the peak heat-flux may be even greater than that of the circular leading-edge (Figure 17, Table 7). But then, as presented in Table 7, the peak value can be efficiently decreased by more than 4% if the attack angle is no greater than 15°. To sum up, the optimal leading-edge can efficiently reduce the peak value of heat-flux in a wide range of attack angle.

Table 7 Comparison of peak heat-flux for various attack angle values

Attack angle	Baseline	Optimal	Reduced by
0°		3308691.5	+20%
5°		3472969.3	+16%
10°		3715737.3	+10%
15°	4132495.5	3965252.3	+4%
20°		4290240.0	-4%
25°		4781591.5	-16%
30°		5344462.0	-29%

V. Axisymmetric Cases

The optimal profile of leading-edge has indeed good robustness as discussed in §IV. The peak value of heat-flux can be efficiently reduced by using the optimal leading-edge in all these cases.

For the blunt revolution body (axisymmetric body), it exhibits a similar heat-flux distribution as that of the 2-D cylinder leading-edge (theoretical self-similar solutions[17-21, 24]). And J.D. Anderson etc. [21] pointed out that the heat-flux at the stagnation point of axisymmetric bodies also follows Equation (5). Accordingly, the optimal 2-D profile can also be used for revolution blunt bodies (nose-tip) to reduce the peak value of heat flux as the curvature radius in the vicinity of stagnation point increases greatly. To verify the aero-thermal protection performance of the

optimal axisymmetric model, five cases are selected, with parameters given in Table 8, by referring to the principle of maximum range of unit Reynolds number and the cases chosen in §IV.

As for the circular cone and the optimal axisymmetric model, the peak heat-flux of the optimal cases is effectively reduced by 25%~30%, though the drag coefficients are increased by 24%~30% (Table 9). The results for different flight Mach numbers (Case1/Case2), flight altitudes (Case1/Case3/Case4) and thickness of the nose-tip (Case1/Case5) are analyzed too. All these cases show good performance in reducing peak heat-flux as compared to the corresponding case of circular cone. Reasonably, it's feasible and reliable to reduce the peak heat flux of blunt bodies by using the optimal 2-D profile.

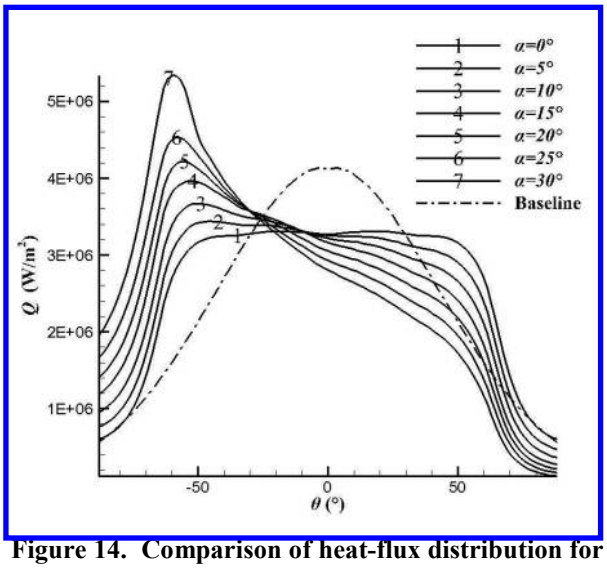

Figure 14. Comparison of heat-flux distribution for various attack angles.

Table 8 Axisymmetric cases

CASES	T_w(K)	Ma_∞	Altitude(Km)	Thickness(mm)	$Re_\infty(m^{-1})$
Case1		6.5	25	5	5.28E+06
Case2		10	25	5	8.13E+06
Case3	300	6.5	20	5	1.19E+07
Case4		6.5	40	5	4.96E+05
Case5		6.5	25	40	5.28E+06

Table 9 Comparison of peak heat-flux and drag coefficient for axisymmetric cases

Q_{max}/F_{drag}	CASES	Baseline	Optimal	Reduced by
Q_{max} (W/m^2)	Case1	6067267.5	4421479.0	+27%
	Case2	23695396.0	17258988.0	+27%
	Case3	8792375.0	6534553.0	+26%
	Case4	2519911.8	1772581.4	+30%
	Case5	2252440.0	1692209.9	+25%
Drag coefficient	Case1	0.2336	0.3005	-29%
	Case2	0.2315	0.2998	-30%
	Case3	0.2813	0.3480	-29%
	Case4	0.2274	0.2933	-24%
	Case5	0.8980	1.1601	-29%

Compared to the 2-D cylinder cases, the shock stand-off distance of the axisymmetric model decreases dramatically, and the temperature gradient within the thermal boundary layer and surface heat-flux of the cone increases greatly as the thickness of thermal boundary layer has been compressed thinner (Table 2, Table 9). As compared to the circular cone, the thermal boundary layer thickness of the optimal cone is increased by about 45% (from 2.9×10^{-5}m to 4.2×10^{-5}m, as shown in Figure 20). Besides, the heat-flux is similarly characterized with uniform distribution in the zone of $|\theta|\in(0°,50°)$(Figure 18). For the ablative thermal protection technology, the proposed profile is helpful for the flight control as the material of nose-tip is uniformly ablated.

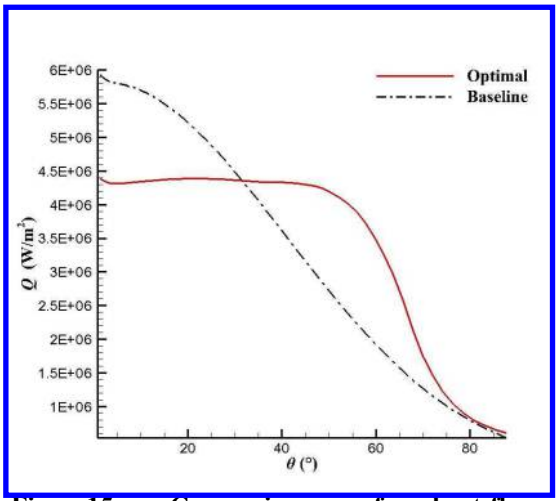

Figure15. Comparison of heat-flux distribution for Case 1.

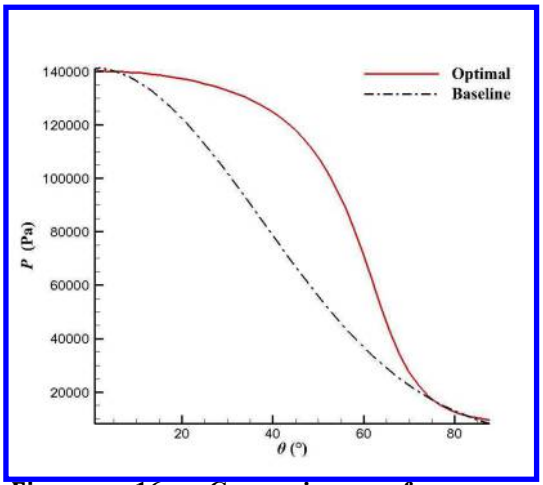

Figure 16. Comparison of pressure distribution for Case 1.

VI. Summary and Conclusions

Based on the numerical simulation, the Mini-Max optimization model has for the first time been adopted to minimize the peak heat flux of hypersonic vehicles' leading-edge, and an optimal 2-D profile with reasonable curvature distribution is obtained. For the optimal 2-D profile, it is characterized with greater curvature radius in the vicinity of the stagnation point (for the zero-incidence flow), and smaller curvature radius in the zone of $|\theta| \in (50°,80°)$ where the aero-heating is not that serious as in the vicinity of stagnation point. With the circular leading-edge as Baseline, the optimal one seems to be 'blunter', the high temperature and high pressure area downstream of the shock wave is enlarged, and the surface temperature and pressure increase in the vicinity (except the stagnation point) of the stagnation point. On the other side, the shock stand-off distance increases, and the thickness of the thermal boundary layer is increased (increased by about 40% at the stagnation point). As a result, the temperature gradient within the thermal boundary layer decreases, and the peak value of heat-flux is reduced by about 20% accordingly. Besides, the heat-flux is characterized with nearly uniform distribution in the zone of $|\theta| \in (0°,50°)$, which means that it is uniformly heated in the most serious aero-heating areas. And this distribution character would help to keep the geometry shape unchanged if the ablative thermal protection technology is adopted.

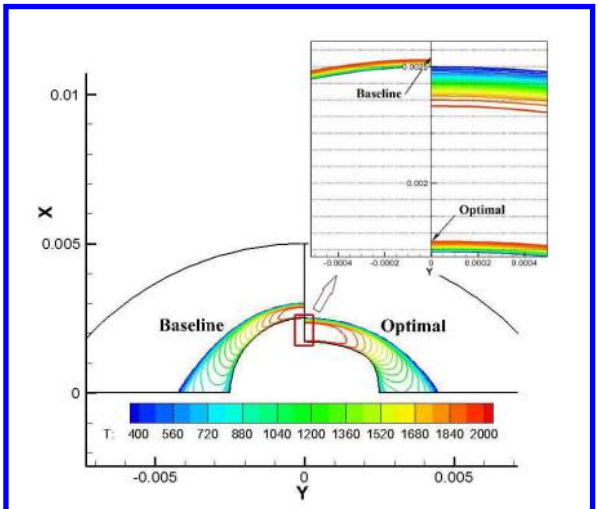

Figure 17. Comparison of temperature contours and thickness of thermal boundary layer for axisymmetric cases.

The robustness of the optimal leading-edge has been discussed in details in §IV, and the factors that may impact the peak heat-flux are individually analyzed. For different wall temperature T_w, flight altitude H, flight Mach number Ma_∞ and thickness of leading-edge D (the optimal and circular profiles need be scaled to meet the size of thickness), the peak heat-fluxes are all effectively reduced by about 20% and characterized with nearly uniform heat-flux distribution in the zone of $|\theta| \in (0°,50°)$. The peak heat-flux of the optimal leading-edge increases as the flight attack angle α increases, and the peak value is located in the zone of $|\theta| \in (60°,70°)$ which is characterized with smaller curvature radius. Even so, the peak heat-flux would be decreased by more than 4% if the attack angle isn't greater than 15°. In other words, the optimal leading-edge can effectively reduce the peak heat-flux in a wide range of angle of attack. In addition, the optimal 2-D profile has been proposed in §V to be used to generate an axisymmetric model. As compared to the corresponding circular cone, the peak heat-flux of the optimal cone can effectively be reduced by about 25%~30% (there is a little difference between the selected five cases). Similarly, the heat-flux distribution of the optimal cone is nearly uniform in the vicinity of the stagnation point.

The numerical results in this paper also show an obvious increase of drag coefficient as the peak heat-flux decreases. The drag coefficient is increased by about 12% (Table 2) at the design point for 2-D cylinder model, and it is increased even greater for the axisymmetric model (increased by about 24%~30% as compared to the corresponding circular cone, as shown in Table 9). However, the thickness of the leading-edge is taken as the reference area of the drag coefficient in this paper. The size of the leading-edge is much smaller than that of the whole vehicles, and drag of the leading-edge is a quite small part of the total drag of the vehicle. For the effects of the novel direct blunting method on the aerodynamic performance of hypersonic vehicles, subsequent study will soon be carried out.

Acknowledgments

The support of the National Natural Science Foundation of China (Grant No. 90916013) is gratefully acknowledged.

References

1. Nonweiler, T.R.F., "Aerodynamic problems of manned space vehicles," Journal of the Royal Aeronautical Society, Vol. 63, No.4, 1959, pp. 521-528
2. Bowcutt, K.G., Anderson J.D., and Capriotti D., *Numerical optimization of conical flow waveriders including detailed viscous effects*, Defense Technical Information Center, 1987
3. Cui, K., Zhao D.X., and Yang G.W., "*Waverider configurations derived from general conical flowfields*," Acta Mechanica Sinica, Vol. 23, No.3, 2007, pp. 247-255
4. Maull, D.J., "*Hypersonic flow over axially symmetric spiked bodies*," Journal of Fluid Mechanics, Vol. 8, No.04, 1960, pp. 584-592
5. Wood, C.J., "*Hypersonic flow over spiked cones*," Journal of Fluid Mechanics, Vol. 12, No.04, 1962, pp. 614-624
6. Ahmed, M.Y.M. and Qin N., "*Recent advances in the aerothermodynamics of spiked hypersonic vehicles*," Progress in Aerospace Sciences, Vol. 47, No.6, 2011, pp. 425-449
7. Warren, C.H.E., "*An experimental investigation of the effect of ejecting a coolant gas at the nose of a bluff body*," Journal of Fluid Mechanics, Vol. 8, No.03, 1960, pp. 400-417
8. Finley, P.J., "*The flow of a jet from a body opposing a supersonic free stream*," Journal of Fluid Mechanics, Vol. 26, No.02, 1966, pp. 337-368
9. Chen, L.W., Wang G.L., and Lu X.Y., "*Numerical investigation of a jet from a blunt body opposing a supersonic flow*," Journal of Fluid Mechanics, Vol. 684, No.1, 2011, pp. 85-110
10. Johnson, R.H., "*Instability in hypersonic flow about blunt bodies*," Physics of Fluids, Vol. 2, No.5, 1959, pp. 526-532
11. Bohachevsky, I.O. and Kostoff R.N., "*Supersonic flow over convex and concave shapes with radiation and ablation effects*," AIAA Journal, Vol. 10, No.8, 1972, pp. 1024-1031
12. Silton, S. and Goldstein D., "*Ablation onset in unsteady hypersonic flow about nose tip with cavity*," Journal of Thermophysics and Heat Transfer, Vol. 14, No.3, 2000, pp. 421-434
13. Silton, S.I. and Goldstein D.B., "*Use of an axial nose-tip cavity for delaying ablation onset in hypersonic flow*," Journal of Fluid Mechanics, Vol. 528, 2005, pp. 297-321
14. Driest, E.R.V., "*The problem of aerodynamic heating*," Aeronautical Engineering Review, Vol. 15, No.10, 1956, pp. 26-41
15. Lees, L., "*Laminar heat transfer over blunt-nosed bodies at hypersonic flight speeds*," Journal of Jet Propulsion, Vol. 26, No.4, 1956, pp. 259-269
16. Fay, J.A. and Riddell F.R., "*Theory of stagnation point heat transfer in dissociated air*," Journal of the Aeronautical Sciences, Vol. 25, 1958, pp. 73-85
17. Kemp, N.H., Rose P.H., and Detra R.W., "*Laminar heat transfer around blunt bodies in dissociated air*," Journal of the Aeronautical Sciences, Vol. 26, No.7, 1959, pp. 421-430
18. Rose, P.H. and Stark W., "*Stagnation point heat transfer measurements in dissociated air*," Journal of the Aeronautical Sciences, Vol. 25, No.2, 1958, pp. 86-97
19. Rose, P.H. and Stankevics J.O., "*Stagnation point heat transfer measurements in partially ionized air*," AIAA Journal, Vol. 1, No.12, 1963, pp. 2752-2763
20. Marvin, J.G. and Deiwert G.S., *Convective heat transfer in planetary gases*, National Aeronautics and Space Administration, 1965doi:10.2514/3.3523
21. Sutton, K. and Graves R.A., *A general stagnation-point convective-heating equation for arbitrary gas mixtures*, National Aeronautics and Space Administration, 1971
22. Anderson, J.D., *Hypersonic and high temperature gas dynamics*, American Institute of Aeronautics and Astronautics, 2006doi:10.2514/4.861956
23. Younis, A. and Dong Z., "*Trends, features, and tests of common and recently introduced global optimization methods*," Engineering Optimization, Vol. 42, No.8, 2010, pp. 691-718
24. Tauber, M.E., *A review of high-speed, convective, heat-transfer computation methods*, National Aeronautics and Space Administration, 1989